Deriving Thermospheric Winds from Distributed Fabry-Perot Arrays

M. Conde[1], C. Anderson[1] , M. G. McHarg[2] [[1]Geophysical Institute, University of Alaska Fairbanks; [2]US Air Force Academy]

Geophysical Institute
University of Alaska Fairbanks

Abstract

Fabry-Perot spectrometers have been used since the 1960's for ground based remote sensing of thermospheric winds. However, because the technique only measures the wind's line of sight component, it is not possible to infer even the 2-component horizontal wind field from observations recorded by a single instrument, unless substantial assumptions are made. The obvious way to overcome this limitation is to deploy an array of instruments at two or more geographic locations. It is then possible to derive unambiguous estimates of two or even all three wind components, for atmospheric regions that are viewed by the array along multiple non-colinear look directions. Here we use this approach to derive winds from an array of three all-sky Fabry-Perot spectrometers in Alaska. However, the geographic regions where the viewing geometry is favorable for this direct approach are surprisingly limited. As an alternative, we also present winds derived from least-squares fitting of 2-component polynomial basis functions to the line-of-sight wind data. Although this second technique is locally less accurate than the direct approach, it is also less sensitive to measurement noise, and it does provide a complete uninterrupted wind field throughout the geographic region spanned by the measurements. Results of both methods are compared.

Fabry-Perot Measurements of Thermospheric Winds

In the mid 1990's the University of Alaska's Geophysical Institute developed a new type of Fabry-Perot spectrometer for remote sensing thermospheric wind and temperature fields. Installed at Poker Flat in Alaska and dubbed the "Scanning Doppler Imager" (SDI), its salient features included a low-light imaging detector with high time resolution, a capacitance-stabilized etalon capable of piezo-electric separation scanning at $5\,\mathrm{Hz}$ or faster, and wide-angle fore optics arranged to place a sharp image of the sky onto the detector [*Conde & Smith*, 1995, 1997, 1998]. The instrument resolves the sky scene into a software-defined set of sub-regions, and compiles a high-resolution Doppler spectrum of the source illumination originating from each one. These spectra, typically span a wavelength interval of around $10\,\mathrm{pm}$, and are used to infer Doppler shifts and Doppler widths of the illumination, which are in turn used to infer winds and temperatures at the height of the atmospheric optical emission layer. In recent versions of these instruments the field-of-view is typically divided into 115 sub-regions, and it extends from the zenith down to about 25° to 30° elevation angle. Thus, when observing the $630\,\mathrm{nm}$ emission, winds and temperatures are measured in a region that is around $1100\,\mathrm{km}$ in diameter. The SDI instruments, like all Doppler spectrometers, can only measure the line-of-sight component of the wind vector that prevails in the region of atmosphere from which the emission originates. However, most aeronomic applications require knowledge of at least the two-component horizontal wind field or, possibly complete three-component winds. This poster therefore compares several strategies for deriving estimates of vector winds, based on the line-of-sight measurements produced by Fabry-Perot spectrometers.

Monostatic Wind Measurments

Consider a single instrument observing the sky a a fixed (but not small) zenith angle, and in n different azimuths that are equally-spaced and span a full 360°. We obtain estimates of the horizontal vector wind field from the observed line-of-sight wind components by fitting a two-component field that has first-order dependence on geographic position with the form We approximate the total horizontal vector wind field using first-order Taylor series expansions of the zonal and meridional components about the zenith,

$$H_x = u_0 + \frac{\partial u}{\partial x}x + \frac{\partial u}{\partial y}y$$

$$H_y = v_0 + \frac{\partial v}{\partial x}x + \frac{\partial v}{\partial y}y,$$

where u and v are the zonal and meridional wind components, and x and y are the zonal and meridional distances from the observatory to an observation point viewed at zenith angle θ and azimuth angle ϕ. That is,

$$x = R\sin\phi$$

$$y = R\cos\phi$$

$$R = h\tan\theta,$$

with h being the height of the emission layer. The vector wind field can thus be obtained if the line-of-sight data can be used to derive values for the six coeficients that appear in this model, i.e., u_0, v_0, $\frac{\partial u}{\partial x}$, $\frac{\partial u}{\partial y}$, $\frac{\partial v}{\partial x}$ and $\frac{\partial v}{\partial y}$. In practice, we only use this fitted wind field at each viewing location to describe the horizontal wind component that is oriented perpendicular to our line-of-sight. The parallel horizontal components are retained from the original line-of-sight measurements.

To derive the model coefficients, we first subtract the contribution of the vertical wind (estimated from zenith observations) from the line-of-sight wind in each viewing direction. We then fit the observed "horizontal only" line-of-sight data $H^{\parallel}(\phi,\theta)$ with a Fourier series of the form

$$H^{\parallel}(\phi,\theta) = \{a_0 + \sum_{m=1}^{\frac{n}{2}-1}(a_m\sin m\phi + b_m\cos m\phi)\}\sin\theta.$$

The required Fourier coefficients are easily found using standard methods. It is then easily shown [*Conde & Smith*, 1998] that the unkown terms in our linear vector wind model are simply related to the $m = 0, 1,$ and 2 coefficients of the Fourier expansion. However, because there is no meaningful phase associated with the $m = 0$ Fourier terms, there are only five unique Fourier coefficients for the terms up to $m = 2$, whereas the wind model contains six unknowns. This means that an additional constraint is needed to fit the model uniquely.

Burnside et al. [1981] obtained an additional constraint by using information from several consecutive exposures, and assuming that at least over short time intervals

$$\frac{\partial v}{\partial x} \simeq -\frac{1}{\varepsilon}\frac{\partial v}{\partial t},$$

where ε is the tangential velocity of the observatory due to the rotation of the Earth. The assumption is that for sufficiently short time intervals the rotation of the Earth can be regarded as moving the station through a meridional wind field that is stationary in local time. This allows the meridional wind to be sampled at various locations along the zonal direction, which is not possible using line-of-sight data from a single observation.

We have used this "Burnside method" extensively to derive vector winds from SDI data, mostly with good results. However, experience shows the assumption of local-time stationarity of the wind field can (unsurprisingly) be severely violated during times of dynamic forcing, in which case large artifacts occur in the derived wind fields. These mostly appear as spurious eastward or westward traveling vortices. Thus, noting that $\frac{\partial v}{\partial x}$ is in practice normally the weakest of the four first-order gradients, recent versions of our routine analysis simply set it to zero. *Anderson et al.* [2012] showed that although this is actually not a very good assumption, it has surprisingly little impact on the accuracy of our derived vector winds.

Figure 1 presents examples of wind fields derived from this monstatic analysis of data from three SDI instruments in Alaska, located at Toolik Lake, Poker Flat, and HAARP (Gakona). Note that the fitted wind fields are relatively smooth, and that there is broad agreement between the three instruments. But there are also quite significant disagreements in both wind magnitude and wind direction in some places.

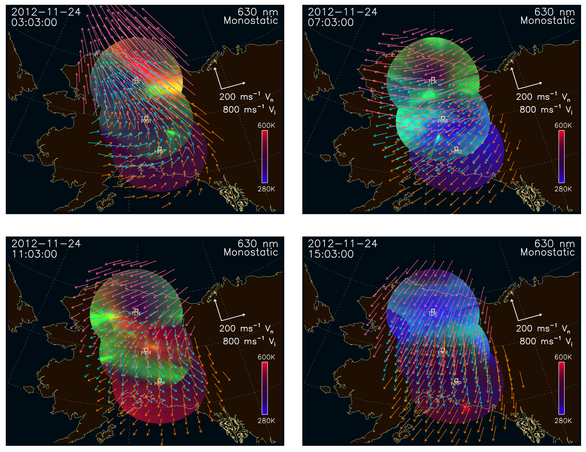

***Figure 1**: Four examples of winds derived from monostatic analysis of spectra from all-sky Fabry Perot instruments located at Toolik Lake (pink arrows), Poker Flat (blue arrows), and HAARP (orange arrows). Green hues in the background images depict auroral brightness at $558\,\mathrm{nm}$, as observed by ground-based all-sky cameras at Poker Flat and Toolik Lake. The cameras images have been projected onto the map assuming the emission comes from a layer located at $120\,\mathrm{km}$ above the surface of the spherical Earth. Blue through red hues depict Doppler temperatures derived from Fabry-Perot spectra of the auroral $558\,\mathrm{nm}$ emission, according to the color scale shown. These temperatures are a proxy for the charatceristic energy of the auroral precipitation, with cooler colors indicating higher energies.*

Bistatic Wind Measurements

For geographic locations that are viewed along non-parallel lines-or-sight by three separate instruments, it is possible to directly estimate all three wind components. We refer to this as using "tristatic" observations and analysis to derive wind estimates. Conversely, in locations with only two independent lines of sight, we can obtain much more direct estimates of two wind components. We refer to this as the "bistatic" method, and our approach to it has been described in detail by *Anderson et al.* [2012a; 2012b; 2012c]. Briefly, the steps in the analysis are:

1. Temporally interpolate the line-of-sight wind data from each observatory onto a set of common observing times.
2. Identify pairs of viewing zones with at least 10% overlap in area when projected onto the emisison layer.
3. Select subsets of the overlapping zone pairs for which the viewing geometry is suitable for obtaining direct estimates of the vertical wind component. In practice, this means finding overlapping zone pairs located along the great-circle path defined by the two observatories.
4. Derive estimates of the vertical wind at each common time from these zone pairs.
5. Extrapolate the vertical wind estimates to all viewing zone locations and, for each common time, subtract the line-of-sight component of the vertical wind from all line-of-sight wind data. This yields estimates of the line-of-sight component of the horizontal wind field alone.
6. Select subsets of the overlapping zone pairs for which the viewing geometry is suitable for obtaining direct estimates of the two horizontal wind components. In practice, this selects clusters of zone pairs that are located either side of the great circle path. For each of these pairs, identify common times when line-of-sight wind uncertainties are small enough to indicate good data.
7. For each zone pair and time identified in step 6, use simple trigonometry to estimate the two components of the horizontal wind.

Unfortunately, the sites chosen for our three existing Alaskan all-sky Fabry-Perot instruments were driven mostly by logistic considerations – each is located on Alaska's very limited road system. This means the current array is almost colinear, which means tristatic analysis is not yet possible. (We should soon add a 4th site at Kaktovik, which will allow extensive tristatic analysis.)

Thus, Figure 2 shows results of bistatic wind analysis of data for the same times (and in the same format) as the monostatic analyses shown in Figure 1. Note the limited geographic regions that are suitable for this analysis. However, within these regions more complex structure is resolved in the wind field. These results are also noisier, because each arrow is derived from just two overlapping zones, whereas the other procedures shown here essentially produce winds that are a "best fit" to data from large numbers of zones.

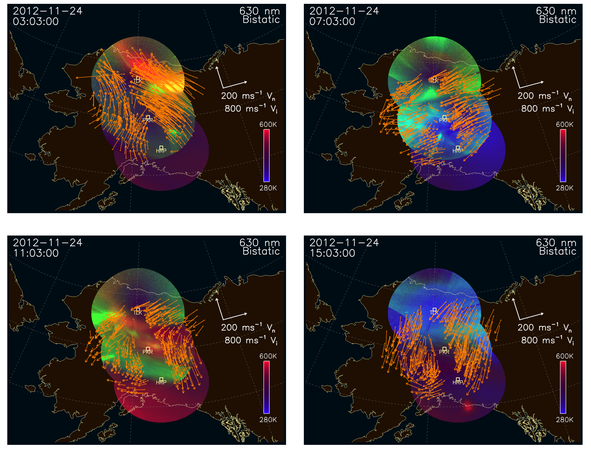

***Figure 2**: Four examples of winds derived from bistatic analysis of spectra from the Alaskan all-sky Fabry-Perot array. Times and presentation format are as per Figure 1.*

Multistatic Wind Measurements

Of our techniques for processing data from the Alaskan SDI array, we regard results from direct bistatic fitting as the "gold standard", in the sense that it is the most direct method currently available, and it requires the least assumptions. However, as noted, the results can be noisy, and they are only available in limited geographic regions. We have thus developed a hybrid approach, in which the line-of-sight winds from all three stations are fitted simultaneously to a two-component low-order polynomial wind model. Further, a form of inverse-distance weighting is used to localize the fits (to some degree) about each particular location for which a final wind estimate is required. This means that the fit coefficients are allowed to vary slowly with position as the wind estimate location moves around.

For this analysis we approximate the vector wind field using k–th order Taylor series expansions of the zonal, meridional, and vertical components about some convenient reference location, i.e.

$$\begin{aligned}
u &= u_0 + \frac{\partial u}{\partial x}x + \frac{\partial u}{\partial y}y + \frac{\partial^2 u}{\partial x^2}x^2 + \frac{\partial^2 u}{\partial x\partial y}xy + \frac{\partial^2 u}{\partial y^2}y^2 + \ldots + \frac{\partial^k u}{\partial x^k}x^k + \frac{\partial^k u}{\partial x^{k-1}\partial y}x^{k-1}y + \frac{\partial^k u}{\partial y^k}y^k \\
v &= v_0 + \frac{\partial v}{\partial x}x + \frac{\partial v}{\partial y}y + \frac{\partial^2 v}{\partial x^2}x^2 + \frac{\partial^2 v}{\partial x\partial y}xy + \frac{\partial^2 v}{\partial y^2}y^2 + \ldots + \frac{\partial^k v}{\partial x^k}x^k + \frac{\partial^k v}{\partial x^{k-1}\partial y}x^{k-1}y + \frac{\partial^k v}{\partial y^k}y^k \\
w &= w_0 + \frac{\partial w}{\partial x}x + \frac{\partial w}{\partial y}y + \frac{\partial^2 w}{\partial x^2}x^2 + \frac{\partial^2 w}{\partial x\partial y}xy + \frac{\partial^2 w}{\partial y^2}y^2 + \ldots + \frac{\partial^k w}{\partial x^k}x^k + \frac{\partial^k w}{\partial x^{k-1}\partial y}x^{k-1}y + \frac{\partial^k w}{\partial y^k}y^k
\end{aligned}$$

where x and y are distances east and north from our reference location.

From this we can calculate an n-element vector describing the line-of-sight components that would be seen at each of the n viewing locations if our Fabry-Perot array was observing the model wind field. (Note that we are using the term "vector" here in the mathematical sense rather than a physical vector with magnitude and direction.) We denote this vector as $\mathbf{M}$, and note that its individual elements are simple scalars. $\mathbf{M}$ bears the same relationship to our vector wind field model as our observations, $\mathbf{W}$, bear to thephysical vector wind field prevailing in the atmosphere during the observations. The i-th element of $\mathbf{M}$ is given by

$$\begin{aligned}
m_i \;=\; & u_0\sin\phi_i + v_0\cos\phi_i + w_0\cos\theta_i \\
& \frac{\partial u}{\partial x}x_i\sin\phi_i + \frac{\partial u}{\partial y}y_i\sin\phi_i + \frac{\partial v}{\partial x}x_i\cos\phi_i + \frac{\partial v}{\partial y}y_i\cos\phi_i + \frac{\partial w}{\partial x}x_i\cos\theta_i + \frac{\partial w}{\partial y}y_i\cos\theta_i + \\
& \frac{\partial^2 u}{\partial x^2}x_i^2\sin\phi_i + \frac{\partial^2 u}{\partial x\partial y}xy\sin\phi_i + \frac{\partial^2 u}{\partial y^2}y_i^2\sin\phi_i + \\
& \frac{\partial^2 v}{\partial x^2}x_i^2\cos\phi_i + \frac{\partial^2 v}{\partial x\partial y}xy\cos\phi_i + \frac{\partial^2 v}{\partial y^2}y_i^2\cos\phi_i + \\
& \frac{\partial^2 w}{\partial x^2}x_i^2\cos\theta_i + \frac{\partial^2 w}{\partial x\partial y}xy\cos\theta_i + \frac{\partial^2 w}{\partial y^2}y_i^2\cos\theta_i + \ldots
\end{aligned}$$

Thus, for a k-th order fit, we have $K = 3\Sigma_{i=0}^{k}(i+1)$ model coefficients to fit. We denote these as a vector, $\mathbf{a}$. Writing $\mathbf{a}$ in terms of its individual elements gives

$$\mathbf{a} = \left(u_0,\; v_0,\; w_0,\; \frac{\partial u}{\partial x},\; \frac{\partial u}{\partial y},\; \frac{\partial v}{\partial x},\; \frac{\partial v}{\partial y},\; \frac{\partial w}{\partial x},\; \frac{\partial w}{\partial y},\; \frac{\partial^2 u}{\partial x^2},\; \frac{\partial^2 u}{\partial x\partial y},\; \frac{\partial^2 u}{\partial y^2},\; \frac{\partial^2 v}{\partial x^2},\; \frac{\partial^2 v}{\partial x\partial y},\; \frac{\partial^2 v}{\partial y^2},\; \frac{\partial^2 w}{\partial x^2},\; \frac{\partial^2 w}{\partial x\partial y},\; \frac{\partial^2 w}{\partial y^2}, \ldots\right)$$

For each model coefficient, there is a corresponding basis function. We denote the j-th basis function evaluated for the i-th viewing location as $B_j(x_i, y_i, \phi_i, \theta_i)$. For a given viewing location, there is a K-element vector of basis function values, given by

$$\mathbf{B} = \begin{pmatrix} \sin\phi_i, & \cos\phi_i, & \cos\theta_i & x_i\sin\phi_i, & y_i\sin\phi_i, & x_i\cos\phi_i, & y_i\cos\phi_i, & x_i\cos\theta_i, & y_i\cos\theta_i, \\ x_i^2\sin\phi_i, & x_iy_i\sin\phi_i, & y_i^2\sin\phi_i, & x_i^2\cos\phi_i, & x_iy_i\cos\phi_i, & y_i^2\cos\phi_i, & x_i^2\cos\theta_i, & x_iy_i\cos\theta_i, & y_i^2\cos\theta_i, \quad \ldots \end{pmatrix}$$

Using the previous two definitions, we can now express $\mathbf{m}$ in terms of $\mathbf{a}$ and $\mathbf{B}$ as

$$m(x_i, y_i, \phi_i, \theta_i) = \sum_{j=1}^{K} a_j B_j(x_i, y_i, \phi_i, \theta_i)$$

We determine the optimum choice for the parameters, $\mathbf{a}$, by minimising the χ^2 parameter

$$\chi^2 = \sum_{i=1}^{n}\frac{(w_i - m_i)^2}{\sigma^2}.$$

where w_i is the i-th element of the line of sight wind observations $\mathbf{W}$. We minimise χ^2 by

Additional Considerations

The multistatic algorithm introduced in the previous section can be applied directly as described. However, we modify it in two important ways to optimize our wind retrievals. Firstly, it is found that the near-colinear our particular array can at times make the procedure unstable when fitting to higher than first-order To stabilize the fits, we invoke a form of the "Burnside method" introduced previously. We this by supplying the fit routine with not just the n observations made at a particular time, but also with n observations interpolated to a time shortly before (20 minutes, typically) and another n observations from shortly afterward. The earlier and later data are displaced westward and eastward respectively, by 0.25° of longitude for each minute of time shift. We refer to this as "Burnside stabilization", because it is a simple implementation of the Burnside method. The second modification is that we call the fitting routine separately for each output location at which we want to calculate the fitted wind. In doing so, the fitting routine is instructed to assign more weight to observations that are "close" to the location for which we are calculating the fitted wind. "Close" in this case is described by a Gaussian weighting funtion of distance, with a $1/e$ half-width of a few hundred km, typically.

Figure 3 presents results of the multistatic analysis for the same four times presented previously, although in a slightly different format. In addition to producing spatially resolved estimates of the two-component horizontal wind field, the multistatic procedure also fits the vertical wind, and calculates various gradients of the horizontal wind at each location, including it's four first-order gradients $\frac{\partial u}{\partial x}$, $\frac{\partial u}{\partial y}$, $\frac{\partial v}{\partial x}$, and $\frac{\partial v}{\partial y}$. Figure 3 thus augments the previous presentation format with maps of the fitted vertical wind, vorticity, and divergence. For comparison, we have also superimposed (in orange) winds obtained by direct bistatic fitting. Further, we have overlaid estimates of the horizontal vector velocity of ion convection derived from SuperDARN (yellow) and PFISR (cyan) data.